

Literature Search and Review

Doug Auld, Anton Simeonov, and Craig Thomas

National Institutes of Health, Bethesda, Maryland.

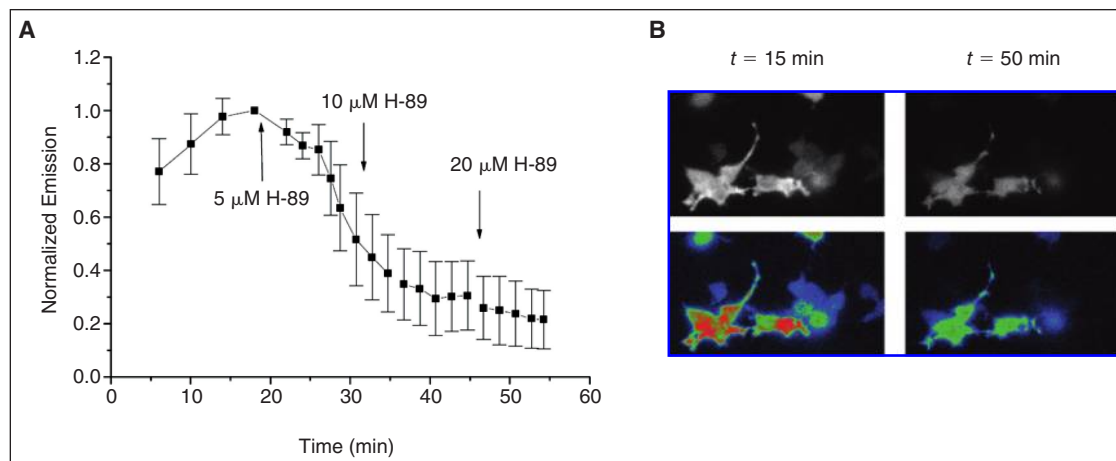
PUZZLING LUCIFERASE INHIBITORS

Herbst KJ, Mallen MD, Zhang J. The cAMP-dependent protein kinase inhibitor H-89 attenuates the bioluminescence signal produced by renilla luciferase. *PLoS ONE* 2009;4:e5642.

Abstract: Investigations into the regulation and functional roles of kinases such as cAMP-dependent protein kinase (PKA) increasingly rely on cellular assays. Currently, there are a number of bioluminescence-based assays, for example reporter gene assays, that allow the study of the regulation, activity, and functional effects of PKA in the cellular context. Additionally, there are continuing efforts to engineer improved biosensors that are capable of detecting real-time PKA signaling dynamics in cells. These cell-based assays are often utilized to test the involvement of PKA-dependent processes by using H-89, a reversible competitive inhibitor of PKA. We present here data to show that H-89, in addition to being a competitive PKA inhibitor, attenuates the bioluminescence signal produced by Renilla luciferase (RLuc) variants in a population of cells and also in single cells. Using 10 μ M of luciferase substrate and 10 μ M H-89, we observed that the signal from RLuc and RLuc8, an eight-point mutation variant of RLuc, in cells was reduced to 50% (\pm 5%) and 54% (\pm 4%) of controls exposed to the vehicle alone, respectively. *In vitro*, we showed that H-89 decreased the RLuc8 bioluminescence signal but did not compete with coelenterazine-h for the RLuc8 active site, and also did not affect the activity of firefly luciferase. By contrast, another competitive inhibitor of PKA, KT5720, did not affect the activity of RLuc8. The identification and characterization of the adverse effect of H-89 on RLuc signal will help deconvolute data previously generated from RLuc-based assays looking at the functional effects of PKA signaling. In addition, for the

current application and future development of bioluminescence assays, KT5720 is identified as a more suitable PKA inhibitor to be used in conjunction with RLuc-based assays. These principal findings also provide an important lesson to fully consider all of the potential effects of experimental conditions on a cell-based assay readout before drawing conclusions from the data

Commentary: Specific inhibition of enzymes used as reporters in high-throughput screening is a concern in early phase compound discovery efforts. Enzymes such as firefly luciferase (FLuc) or Renilla luciferase (RLuc) that catalyze the conversion of small molecule luciferin substrates can be particularly prone to compound inhibition present in chemical libraries. Interferences with these reporters can be on the level of typical hit rates (~1%–5%), thus confusing the identification of compounds active at the desired target in the assay. This article describes the characterization of an RLuc inhibitor, H-89, that is also a well-known inhibitor of PKA. Characterization of H89 involved comparing the activity in cell lines containing a RLuc8 reporter (a stable and brighter luciferase than wild-type RLuc), where the luminescence arose from either a PKA dependent or independent manner. The PKA independent assay was constructed using a cell line expressing RLuc8 and a PKA peptide inhibitor to ensure that PKA was inactivated. Surprisingly, rapid inhibition of RLuc8 luminescence was observed in the PKA independent cell line. RLuc inhibition was confirmed using purified RLuc8 as well as FLuc using K_M levels of luciferin substrates in a defined buffer system (Note: commercial detection reagents should be avoided when determining inhibitor potency against reporter enzymes because these contain high levels of luciferin substrates and the buffer composition is unknown). H-89



H-89 reduces the signal from RLuc8 in single cells. HEK293T cells ($n = 7$) expressing RLuc8 and PKIa were imaged in the presence of 10 μM coelenterazine-h. **(A)** After addition of 5 μM H-89, RLuc8 signal decreases. Additional doses of H-89 decrease the signal further. **(B)** Channel intensity images (top) and pseudocolor images (bottom) of cells corresponding to **(A)** at $t = 15$ min (before H-89 addition) and $t = 50$ min (when signal has reached maximum inhibition).

showed an IC_{50} of 21 μM against RLuc8 but did not show inhibition against the unrelated ATP-dependent enzyme FLuc. Further, H-89 inhibited wild-type RLuc bioluminescence to a similar level. Importantly, the authors show that another reversible PKA inhibitor, KT5720 did not inhibit either forms of RLuc, demonstrating

with the substrate, no covalent adduct was identified in LC-MS experiments. This article should help researchers in examining PKA-dependent pathways in RLuc reporter assays and emphasize the use of appropriate cell lines and counter-screens in cell-based assays. Contributed by Doug Auld.

that KT5720 can be used as an alternative control in RLuc reporter assays where PKA is a component. Currently, the mechanism of inhibition is not completely understood as H-89 shows noncompetitive inhibition. Further, in single cell experiments the inhibition is time dependent (see figure). Although the authors noted a change in the fluorescent spectra when H-89 was incubated with the RLuc substrate coelenterazine-h, suggesting some direct interaction

TYPE SPECIFIC KINASE ASSAY

Simard JR, Klüter S, Grütter C, Getlik M, Rabiller M, Rode HB, et al. A new screening assay for allosteric inhibitors of cSrc. *Nat Chem Biol* 2009;5:394–396.

Abstract: Targeting kinases outside the highly conserved ATP pocket is thought to be a promising strategy for overcoming bottlenecks in kinase inhibitor research, such as limited selectivity and drug resistance. Here we report the development and application of a direct binding assay to detect small molecules that stabilize the inactive conformation of the tyrosine kinase cSrc. Protein X-ray crystallography validated the assay results and confirmed an exclusively allosteric binding mode.

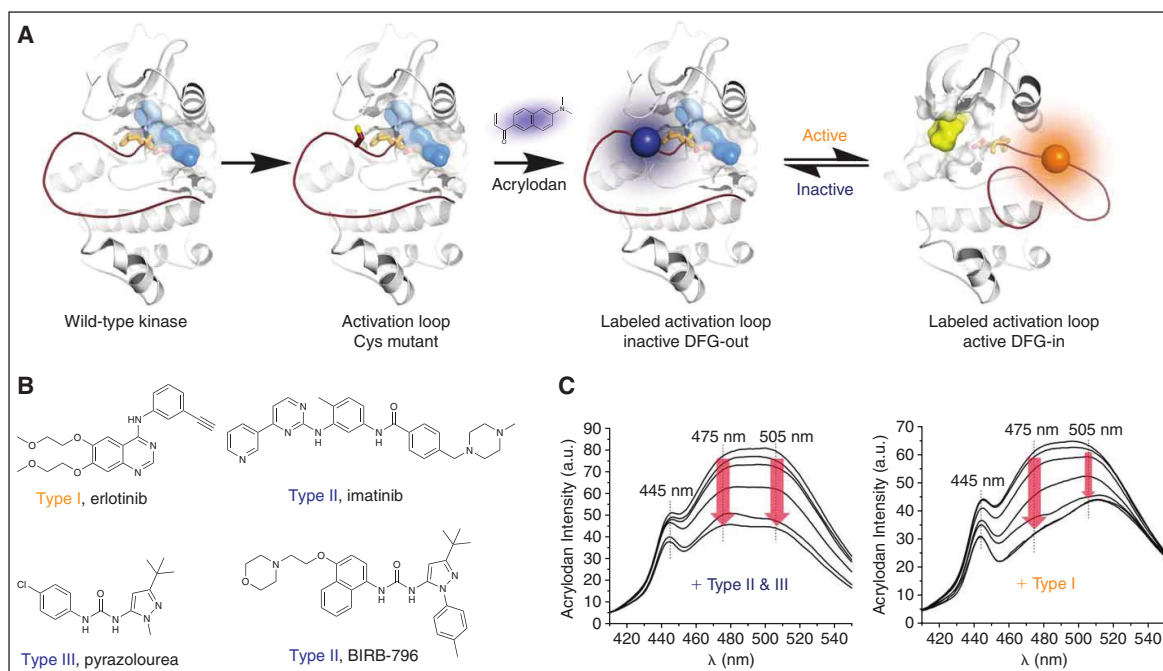
Commentary: Protein kinase inhibitors have been placed in four major categories. Type I inhibitors are competitive with ATP and bind to the kinase by forming a critical hydrogen bond to a hinge region of the kinase domain; Type II inhibitors bind to the same

hinge region but also extend binding interactions to an allosteric pocket that is present only in the inactive form of the kinase; Type III inhibitors do not interact with the hinge region but instead bind only to the allosteric site; and Type IV inhibitors bind outside the ATP binding pocket completely and interact with other regions of the protein kinase. The conformational transition found in many protein kinases that converts the kinase from an inactive to active state involves movement of a phenylalanine residue present in a DFG-motif within the activation loop. The active conformation, known as “DFG-in,” is formed by movement of the phenylalanine side chain into a nearby allosteric pocket. The inactive state, known as the “DFG-out” conformation, has the allosteric pocket open with the phenylalanine side-chain moved away from the pocket. This article describes an assay that is capable of distinguishing between Type I and Type II/III inhibitors by sensing these conformational changes involving the activation loop (see figure). The assay is based on introduction of Cys residue into the activation

LITERATURE SEARCH AND REVIEW

loop and labeling the cysteine residue with acrylodan, an environmentally sensitive fluorophore. (λ_{ex} 386 nm; λ_{em} 450–550 nm). The assay was initially validated with p38 α , a kinase for which Type I, II, and III inhibitors are known. This was then applied to the tyrosine kinase c-Src as no Type III inhibitors are known for this kinase. For the HTS, a 384-well assay was performed where acrylodan was excited at 386 nm and ratiometric fluorescent emission values (445/475 nm) were recorded. This identified four pyrazolourea compounds as weak DFG-out binders, a scaffold known to show nM Type III inhibition of p38 α kinase. Cocrystal structures of these compounds and c-Src were determined that confirmed Type III binding, which appears to be isostructural with

similar cocrystal structures of p38 α kinase. However, the potency of these inhibitors against cSrc was found to be several orders of magnitude weaker than what has been observed for this class of compound against p38 α kinase. The same fluorescent assay was used to examine the kinetics of the interaction. This suggested that a helix that forms the roof of the allosteric pocket is less mobile in cSrc compared to p38 α kinase, which weakens an interaction with a residue known to make hydrogen bonds with the urea scaffold. Therefore, this assay provides both an HTS assay as well as a means to study the mechanism of how compounds effect the conformational transition between inactive and active kinase states. Contributed by Doug Auld.



Schematic diagram of the fluorescent labeled kinase assay for detecting allosteric inhibitors. **(A)** Structural model of a protein kinase of interest with the DFG motif (orange) and activation loop (red) highlighted. A cysteine was mutated into the activation loop of cSrc for subsequent labeling with the environmentally sensitive fluorophore acrylodan to generate a sensitive DFG-out fluorescence-based binding assay. The DFG-out conformation is stabilized by the binding of allosteric type III inhibitors (blue surface representation) or Type II inhibitors that lock the kinase in the inactive state. The binding of ATP or Type I inhibitors (yellow surface representation) stabilizes the active DFG-in conformation. Both conformations are in equilibrium and result from structural changes in the activation loop and the DFG motif. **(B)** Examples of Type I, Type II, and Type III kinase inhibitors and scaffolds. **(C)** In the absence of ligand, acrylodan-labeled cSrc shows two emission maxima at 475 nm and 505 nm. Type I ligands induce a robust loss of fluorescence intensity (red arrows) at 475 nm, resulting in a red shift in the emission maxima to 510 nm (**right panel**). Type II and III inhibitors stabilize the inactive kinase conformation and elicit a different response in which the emissions at 475 nm and 505 nm are equally reduced (**left panel**). The emission signal at 445 nm is less sensitive to ligand binding and serves as an internal reference point, allowing for more stable ratiometric fluorescence measurements and K_d determinations.

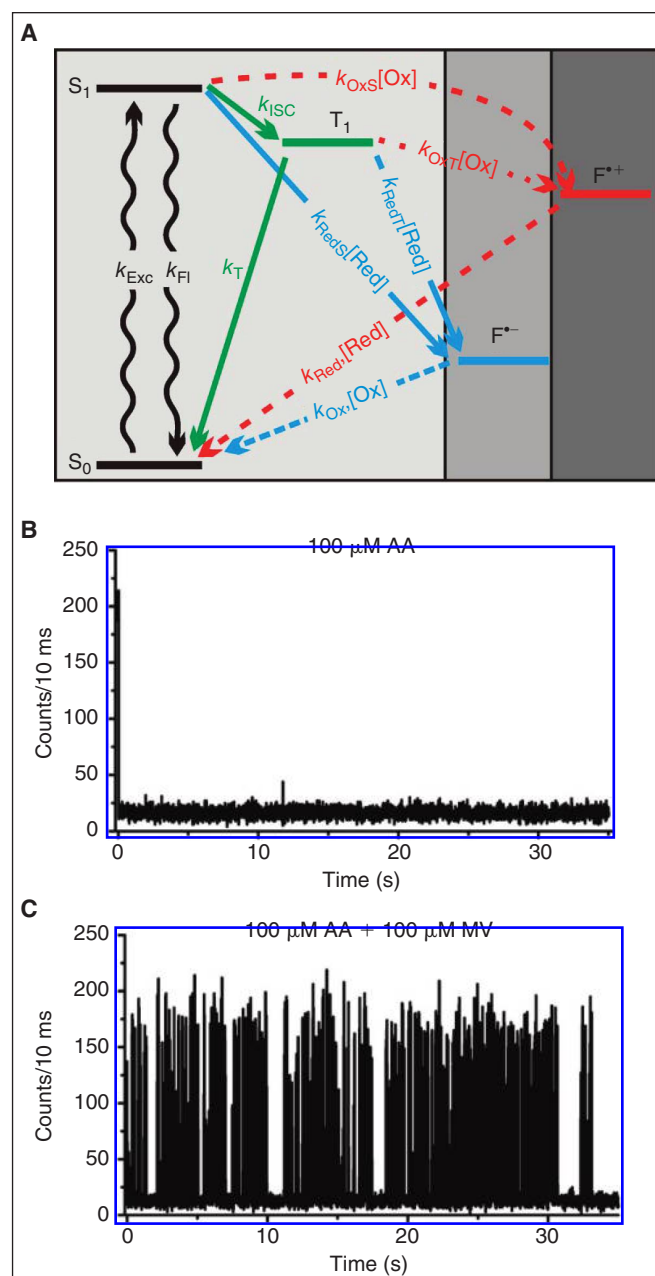
BLINKING FLUOROPHORES

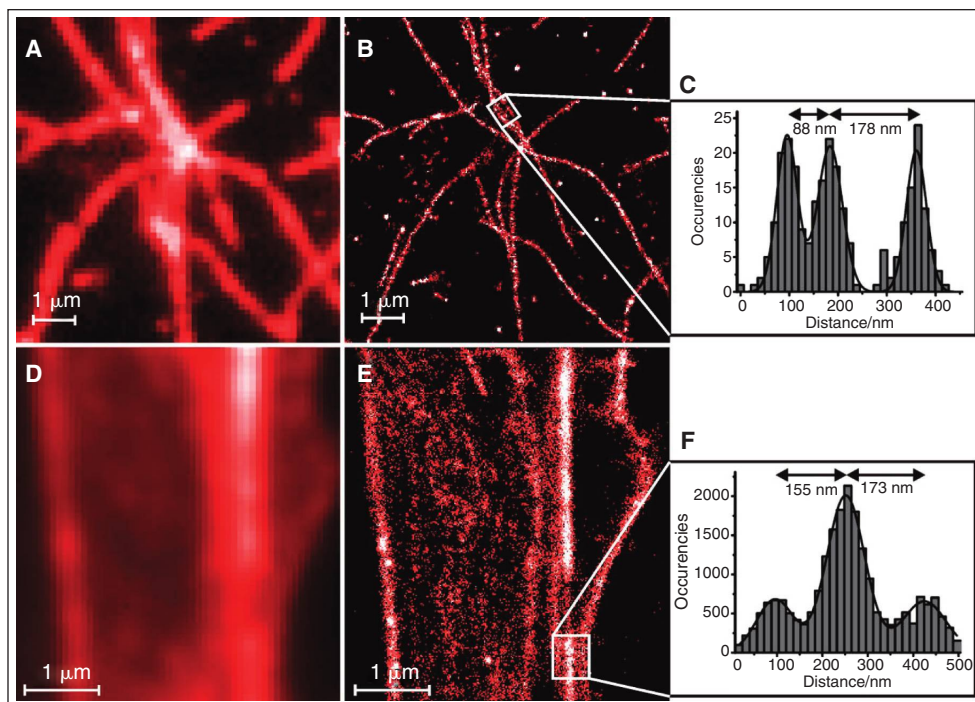
Vogelsang J, Cordes T, Forthmann C, Steinhauer C, Tinnefeld P. Controlling the fluorescence of ordinary oxazine dyes for single-molecule switching and superresolution microscopy. *PNAS* 2009;106:8107–8112.

Abstract: Fluorescent molecular switches have widespread potential for use as sensors, material applications in electro-optical data storages and displays, and super-resolution fluorescence microscopy. We demonstrate that adjustment of fluorophore properties and environmental conditions allows the use of ordinary fluorescent dyes as efficient single-molecule switches that report sensitively on their local redox condition. Adding or removing reductant or oxidant, switches the fluorescence of oxazine dyes between stable fluorescent and nonfluorescent states. At low oxygen concentrations, the off-state that we ascribe to a radical anion is thermally stable with a lifetime in the minutes range. The molecular switches show a remarkable reliability with intriguing fatigue resistance at the single-molecule level: Depending on the switching rate, between 400 and 3,000 switching cycles are observed before irreversible photodestruction occurs. A detailed picture of the underlying photoinduced and redox reactions is elaborated. In the presence of both reductant and oxidant, continuous switching is manifested by “blinking” with independently controllable on- and off-state lifetimes in both deoxygenated and oxygenated environments. This “continuous switching mode” is advantageously used for imaging actin filament and actin filament bundles in fixed cells with subdiffraction-limited resolution.

Photoinduced processes of the fluorophore ATTO655. **(A)** Scheme. After excitation to the first excited singlet state S_1 , fluorescence is emitted at rate k_{Fl} (neglecting nonradiative processes). Intersystem crossing competes with fluorescence and leads to the infrequent formation of triplet states T_1 with the rate constant k_{ISC} . The triplet state is depopulated by intersystem crossing with rate constant k_T or by electron transfer. This may occur either through oxidation by methylviologen (MV) forming a radical cation $F^{\bullet+}$ or through reduction by AA yielding a radical anion $F^{\bullet-}$. The radical ions could be recovered to singlet ground-state fluorophores by the complementary redox reaction. Direct electron transfer from the singlet manifold (k_{RedS} , k_{OxS}) has to be taken into account at higher redox-agent concentration. **(B and C)** Fluorescence transients of ATTO655-labeled dsDNA immobilized in aqueous environment after oxygen removal, addition of 100 μ M AA **(B)** and additionally 100 μ M MV **(C)**, respectively. The transients are binned in 10 ms. Samples were excited at 640 nm with an average excitation intensity of 1.5 kW/cm².

Commentary: Increasing the resolution of microscopes beyond the diffraction limit using fluorescent molecular switches is an important area of research for super-resolution imaging where molecular





Total internal reflection fluorescence microscopy of ATTO655-phalloidin-labeled single actin filaments (A and B) and bundled actin filaments in fixed NIH/3T3 cells (D and E). (A and D) TIRF microscopy images and (B and E) Blink microscopy images with subdiffraction resolution. (C and F) Histograms over the regions marked with a white rectangle in B and E and the corresponding peak to peak distances derived from Gaussian fits. The images were recorded with reductant and oxidant concentrations optimized for imaging speed, fluorophore density, and excitation intensity (see SI Text for details).

structures with sizes \sim nm can be resolved. Currently, fluorescent molecular switches have been applied in imaging, where the switch responds to conditions such as excitation wavelength differences, photon-induced electron transfer, or pH. This article describes the development and characterization of a fluorescent oxazine dyes that shows "blinking" in response to reducing and oxidizes agents. To test the system, biotinylated DNA was labeled with single

oxazine dyes and immobilized to cover slides, which were then treated with a reducing agent (ascorbic acid, AA) or an oxidizing agent (methylviologen, MV). Initially, oxygen was removed from the buffer enzymatically. Placing a single molecule in laser focus and applying AA showed a short fluorescent spike followed by apparent photobleaching. However addition of AA and MV together showed blinking, demonstrating that photobleaching did not occur but that the dark state was due to reduction by AA (see first figure). A detailed characterization of the photo-induced process is presented, where it is shown that all reduced states are long dark states that are rapidly depopulated by MV. Remarkably, MV and AA act independently so that the fluorescent lifetimes of on- and off-states can be controlled over a broad range. The technique was then tested by labeling actin filaments with oxazine fluorophores and recording images using either total internal reflection fluorescent microscopy (TIRF) or "blink microscopy," the latter taking advantage of the short bright on-states and long dark off-states of blinking fluorophores to improve the resolution of the image. The higher resolution of the oxazine-labeled actin filaments with the blink microscope is seen by the ability to resolve three actin bundles not seen with TIRF (see second figure). Further expansion of these fluorophores should provide new redox sensing tools for superresolution microscopes. Contributed by Doug Auld.

DISCOVERING PLURIPOTENT COMPOUNDS

Lyssiotisa CA, Foremanb RK, Staerk J, Garciad M, Mathurb D, Markoulaki S, *et al.* Reprogramming of murine fibroblasts to induced pluripotent stem cells with chemical complementation of Klf4. *PNAS* 2009;06:8912–8917.

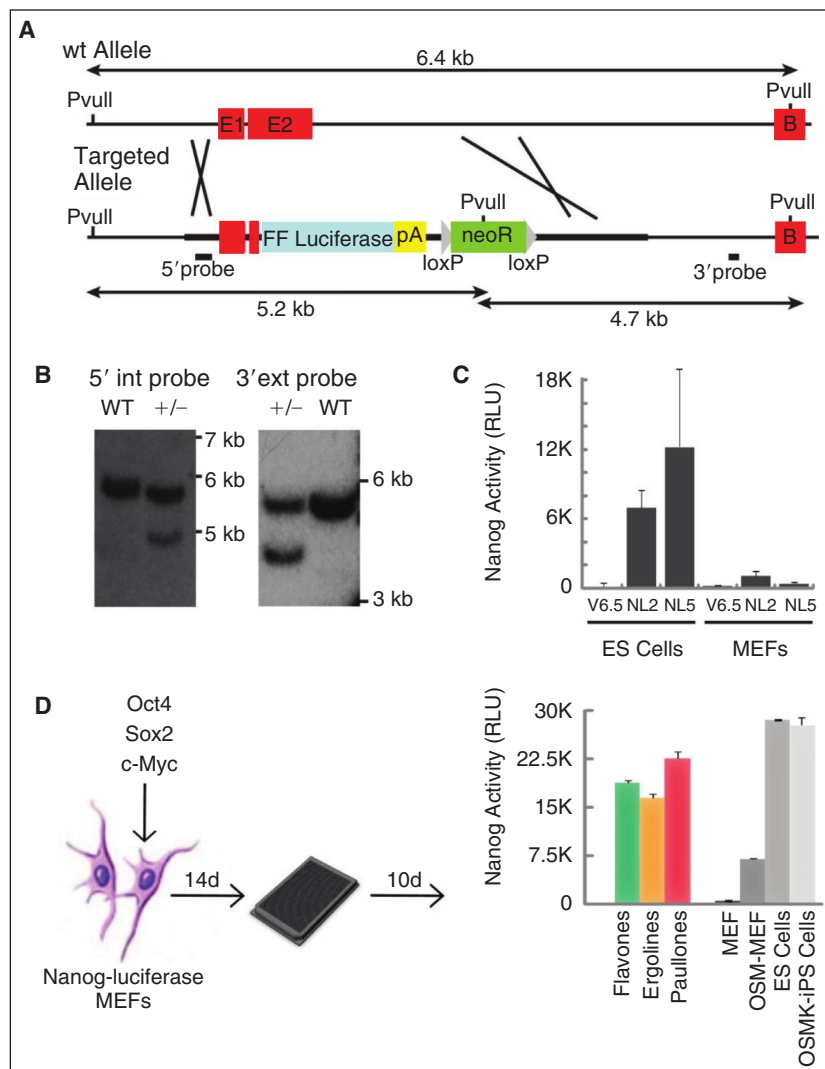
Abstract: Ectopic expression of defined transcription factors can reprogram somatic cells to induced pluripotent stem (iPS)

cells, but the utility of iPS cells is hampered by the use of viral delivery systems. Small molecules offer an alternative to replace virally transduced transcription factors with chemical signaling cues responsible for reprogramming. In this report, we describe a small-molecule screening platform applied to identify compounds that functionally replace the reprogramming factor Klf4. A series of small-molecule scaffolds were identified that activate Nanog

expression in mouse fibroblasts transduced with a subset of reprogramming factors lacking Klf4. Application of one such molecule, kenpaullone, in lieu of Klf4 gave rise to iPS cells that are indistinguishable from murine embryonic stem cells. This experimental platform can be used to screen large chemical libraries in search of novel compounds to replace the reprogramming factors that induce pluripotency. Ultimately, such compounds may provide mechanistic insight into the reprogramming process.

Commentary: Induced pluripotent stem (iPS) cells can be obtained by reprogramming somatic cells through introduction of four transcription factors: Oct4, Sox2, c-Myc, and Klf4; the latter two being oncogenes. Recently, much effort has focused on identifying

small molecules that can enhance or replace these reprogramming factors (see commentary "Pluripotent Small Molecules" *ADDT* 2008;6:743). To screen for small molecules with pluripotent activity this group developed a luciferase reporter gene assay where production of firefly luciferase (FF) was driven by the Nanog promoter (see figure A and B). The Nanog promoter was chosen as this is completely inactivated in somatic cells, and the Nanog transcription factor is one of the master regulators of stem cell pluripotency. To screen for a small molecule replacement of Klf; MEF cells containing the FF reporter were transduced with Oct4, Sox2, and c-Myc and seeded into 1,536-well plates. This led to ~10-fold increase in luciferase activity over nontransduced cells but this activity was still ~4-fold lower than the reporter expressed in pluripotent cells (see figure C and D). Ten days later luciferase activity was measured. After triplicate retesting of hits, approximately 1,000 compounds reproducibly showed >2.5-fold activation of luciferase activity in the assay. These were then subjected to a cell-based counter-screen, where SV40-driven FF expression was used to eliminate compounds that nonspecifically activated the luciferase reporter, which confirmed 135 compounds as genuinely activating the Nanog promoter. The prevalence of luciferase inhibitors that can masquerade as activators in cell-based assay has been estimated to be between 30% and 60% of the actives selected (see *ACS Chem. Biol.*, 2008;3:463-470 and *PNAS* 2009;106:3585-3590). The slightly larger



NL screening platform. (A) Scheme for targeting the firefly (FF) luciferase gene to the Nanog locus. (B) Southern blot hybridization analysis of the NL targeted allele. The targeted allele-specific 5.2-kb and 4.7-kb PvuII fragments were detected with the 5' internal and 3' external probes, respectively, shown in (A). (C) NL activity of correctly targeted ES cell clones (NL2 and NL5) versus NL-MEFs. Differentiated NL tissue shows a significant reduction in luciferase expression. V6.5 ES cells and MEFs are provided as a luciferase negative control. (D) Small-molecule screening strategy. NL-MEFs were transduced with a reduced reprogramming cocktail (Oct4, Sox2, and c-Myc [OSM]), expanded for 2 weeks, plated into 1,536-well plates, treated with compound, and assayed for luciferase expression 10 days after plating: flavones (7-hydroxyflavone, 20 μ M), ergolines (lysergic acid ethylamide, 2' M), and paullones (kenpaullone, 5 μ M). Nanog activity is reported in relative light units (RLUs) and was read in a 96-well (B) or 384-well (D) format. Error bars indicate SD ($n=3$).

LITERATURE SEARCH AND REVIEW

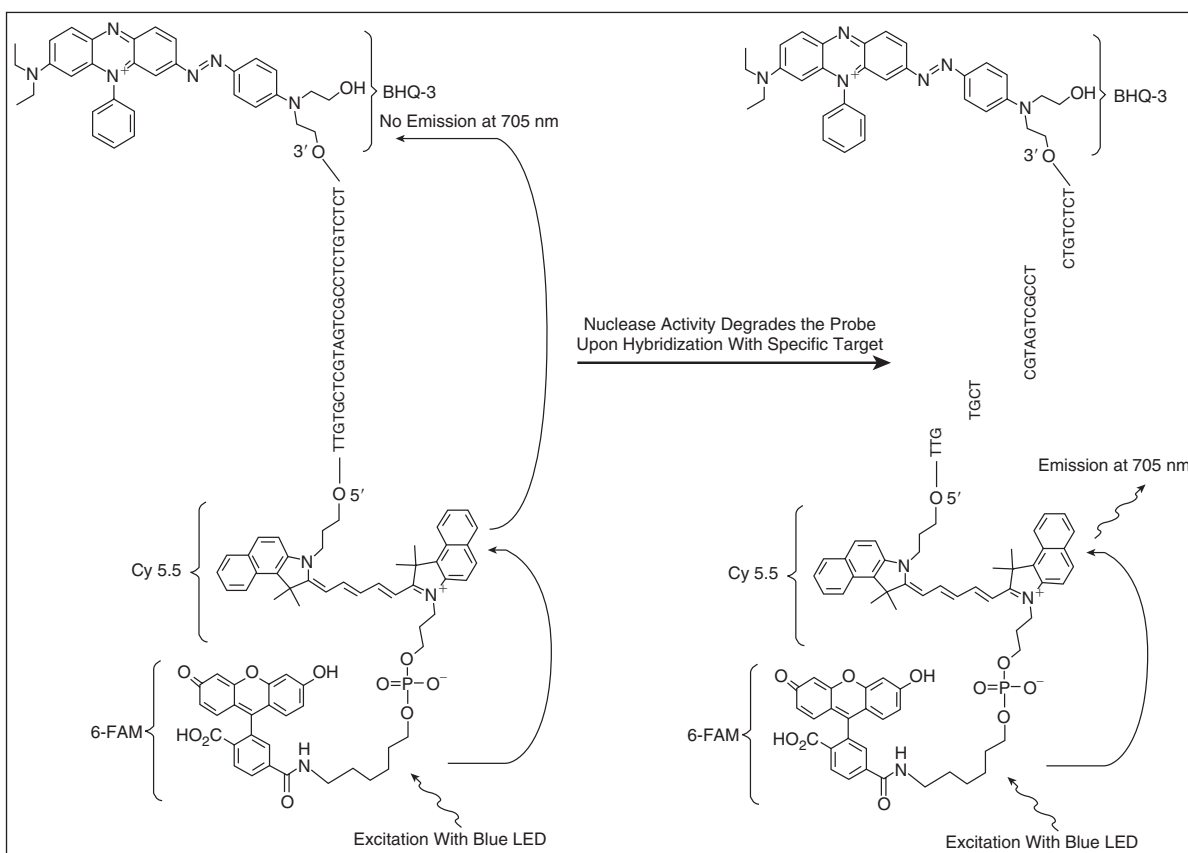
fraction observed by this group (86.5% of the selected hits were eliminated, based on the SV40-FF counter-screen) may be due to the prolonged incubation time in Nanog-FF assay (10 days). Three chemotypes were identified, which included paullones. Secondary assays of colony formation were used to test if these compounds could replace *Klf4* function, which identified Kenpaullone as having pluripotent activity. Kenpaullone is a known inhibitor of sev-

eral kinases including *GSK-3 β* and *CDKs*. However, inhibitors of these kinases could not reproduce the pluripotency of Kenpaullone suggesting a different mechanism is operating in the colony formation assays for this compound. This study demonstrates that small molecule replacements of transcription factors involved with reprogramming can be identified from screening large compound libraries. Contributed by Doug Auld.

WELL-CALIBRATED

Jothikumar P, Hill V, Narayanan J. Design of FRET-TaqMan probes for multiplex real-time PCR using an internal positive control. *BioTechniques* 2009;46:519–524.

Abstract: The multiplexing capabilities with different fluorescent dyes are limited in real-time PCR instruments equipped with one excitation source. Considering this limitation, a design was



Mechanism of wavelength-shifting FRET-TaqMan probe. The FRET-TaqMan probe contains three labels: a black hole quencher moiety at the end of the 3' arm, an emitter fluorophore (Cy5.5), and a harvester fluorophore (FAM) joined together at the end of its 5' arm. The FAM efficiently absorbs energy from blue LED as a light source. In the absence of targets, the probe is dark because the energy absorbed by the FAM is transferred to Cy5.5, and in turn, the energy released from Cy5.5 is transferred to the quencher and is lost as heat energy. In the presence of targets, the TaqMan probe is cleaved by the activity of *Taq* polymerase and quencher is released and the energy absorbed by the FAM is transferred to Cy5.5 through FRET mechanism to emit fluorescence at 705 nm.

developed to create a triple-labeled probe as an internal positive control (IPC) that utilizes a combination of the fluorescence resonance energy transfer (FRET) and TaqMan techniques. The IPC probe, labeled with FAM and Cy5.5 fluorophores at the 5' end and Black Hole Quencher (BHQ) at the 3' end, enabled Cy5.5 emission through energy transfer from the FAM fluorophore. The second, target-specific TaqMan assay in the multiplex used a FAM- and BHQ1-labeled probe at the 5' and 3' ends, respectively. Thus, one excitation source was used to generate two different fluorescence emissions (FAM and Cy5.5) that were measured in two separate channels by the real-time PCR instrument. This method can facilitate the development of a low-cost portable handheld real-time PCR instrument capable of multiplex real-time PCR assays using a single excitation source.

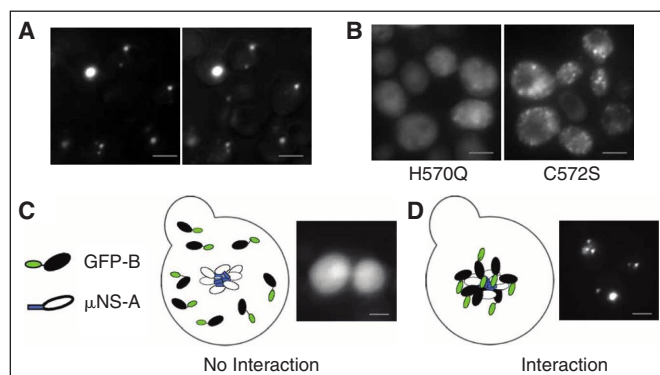
Commentary: The TaqMan probe technology for monitoring allele-specific amplification remains dominant in applications such as real-time PCR and single nucleotide polymorphism (SNP) genotyping. To increase reliability and resolve potential false negatives originating from lack of TaqMan signal due to general inhibition of the amplification reaction (as opposed to absence of the corresponding allele within the sample), internal positive controls are often included during sample preparation. Ideally, such a control should represent a directly adjacent stretch of DNA relative to the typed region. While adding such a template to a sample is relatively easy, its use as an internal standard is often problematic due to the limited signal multiplexing capabilities of many traditional

real-time PCR devices. Jothikumar and colleagues describe a triple-labeled TaqMan probe that can be used in single excitation wavelength devices alongside the regular TaqMan reagents. The probe incorporates a red-shifted Black Hole Quencher (BHQ-3) at its 3' end, and is dual-labeled at the 5' terminus, featuring a fluorescein-Cy5.5 FRET pair (see figure). Blue LED excitation (470 nm) is absorbed by the fluorescein tag, which in turn transfers its energy via FRET mechanism to the adjacent Cy5.5 acceptor; however, in its native state, the probe is dark because the emission from the Cy5.5 label is quenched by BHQ-3. Upon hybridization to its complementary target and during PCR extension, the probe is cleaved to produce a 5' fragment containing the fluorescein-Cy5.5 FRET pair which is no longer quenched by BHQ-3; the signal increase corresponding to this probe can be monitored in the red emission channel (705 nm). At the same time, a probe featuring the traditional 5'-fluorescein-3'BHQ-1 arrangement can be used for the allele-specific detection with fluorescence monitoring in the fluorescein (530 nm) channel. The synthesis of the new probe was achieved with standard phosphoramidite reagents starting with 3' BHQ-3 CPG and ending the oligo sequence with successive incorporations of Cy5.5 and 6-FAM phosphoramidites. Excellent performance of the new probe (no signal from negative control reactions and successful signal separation across multiple emission channels) was noted (Figure 2 of the article). Due to the ease of probe design and synthesis, the present approach to providing an internal standard should find a widespread use. Contributed by Anton Simeonov.

SEE PPI BY PIP

Schmitz AM, Morrison MF, Agunwamba AO, Nibert ML, Lesser CF. Protein interaction platforms: visualization of interacting proteins in yeast. *Nat Methods* 2009;6:500–502.

Abstract: Here we describe the protein interaction platform assay, a method for identifying interacting proteins in *Saccharomyces cerevisiae*. This assay relies on the reovirus scaffolding protein LNS, which forms large focal inclusions in living cells. When a query protein is fused to LNS and potential interaction partners



Development of PIP assay in yeast. (A and B) Yeast cells expressing wild-type (A) or mutant (B) alleles of GFP-μNS at 3–4 h postinduction of fusion protein expression. The left panel in (A) is a fluorescence image; the right panel shows simultaneous imaging of phase and fluorescence illumination. (C and D) Schematic and representative images of PIP. When fused to μNS, protein A is recruited to large platforms. If protein B does not interact with protein A (C), then the localization pattern of protein B is unaltered in the presence of μNS–protein A. Alternatively, if protein B interacts with protein A (D), then a protein B–GFP fusion appears as fluorescent foci. Scale bars are approximately 2 μm.

LITERATURE SEARCH AND REVIEW

are fused to a fluorescent reporter, interactors can be identified by screening for yeast that display fluorescent foci.

Commentary: Despite numerous advances in the field, protein-protein interactions remain difficult to monitor in living cells. The method described here, protein interaction platform (PIP), makes use of a retrovirus scaffolding protein μ NS known to aggregate in the cytoplasm of mammalian cells and to form inclusion bodies detected by microscopy as characteristic foci. The authors present the adoption of the PIP technique to yeast cells where studies of interacting proteins are generally made easier by one's ability to maintain the corresponding protein expression vectors. The detection principle involves making constructs where one of the proteins is fused to μ NS while the other is expressed as a GFP fusion. Thus, cognate interaction between the two proteins results

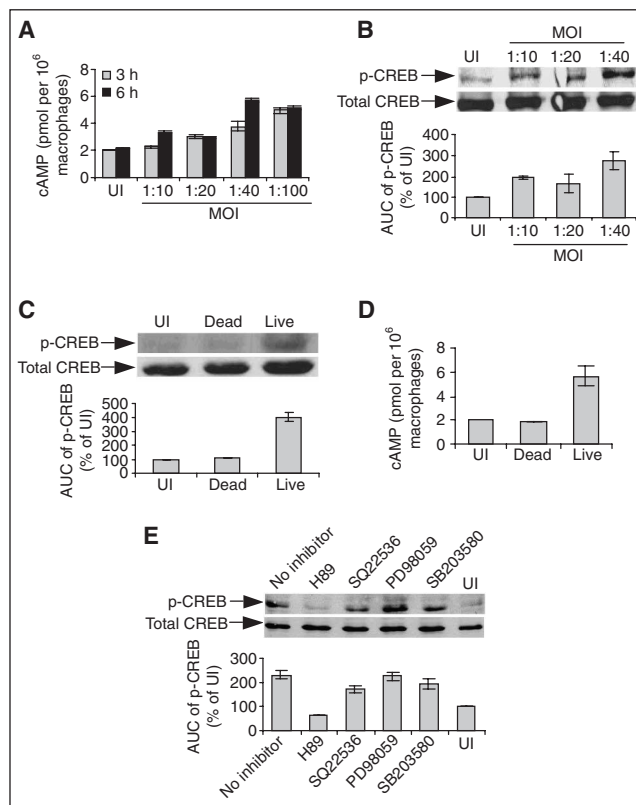
in colocalization of the GFP fluorescence and the μ NS foci (see figure). The μ NS expression and inclusion body formation was shown to be tolerated by the yeast cells and the two protein constructs could be used in either constitutively-expressed or inducible manner. Using this system, the authors demonstrated the interaction between shigella virulence proteins and their secretion chaperones (Figure 2 of the article); the detection outcome was shown to be independent on which particular binding partner was fused to μ NS versus GFP. In addition to simplicity of configuration and use of common light detection methods, the present system is further attractive because it is capable of reporting on protein-protein interactions, regardless of the geometry of the binding. Further validation of the technique as well as the introduction of FRET-type color multiplexing should widen its appeal. Contributed by Anton Simeonov.

CAMP REACH-THROUGH

Agarwal N, Lamichhane G, Gupta R, Nolan S, Bishai WR. Cyclic AMP intoxication of macrophages by a *Mycobacterium tuberculosis* adenylate cyclase. *Nature* 2009;460:98–102.

Abstract: With 8.9 million new cases and 1.7 million deaths per year, tuberculosis is a leading global killer that has not been effectively controlled.^{1,2} The causative agent, *Mycobacterium tuberculosis*, proliferates within the host macrophages, where it modifies both its intracellular and local tissue environment, resulting in caseous granulomas with incomplete bacterial sterilization.^{3,4} Although infection by various mycobacterial species produces a cyclic AMP burst within macrophages that influences

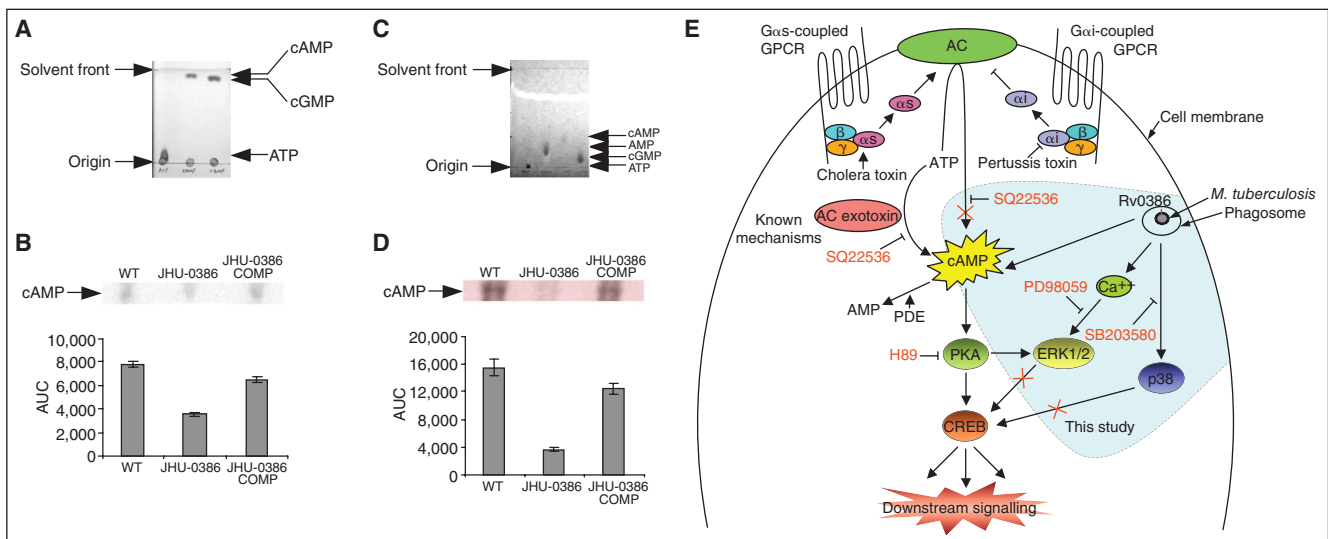
The *M. tuberculosis*-induced macrophage cAMP burst and CREB phosphorylation pathway require live bacilli but not host GPCR-AC. (A and B) Intramacrophage cAMP levels in J774 cells after 3 or 6 h (A) and CREB phosphorylation (p-CREB) after 16 h compared with uninfected (UI) cells (B), at several multiplicities of infection (MOIs). AUC, area under the curve of the densitometric scan. (C and D) Dead (heat-killed) bacilli fail to produce a p-CREB response at 16 h (C) or a cAMP burst at 3 h (D) in J774 cells. (E) Sixteen hour p-CREB accumulation after *M. tuberculosis* infection requires PKA, as shown using the inhibitor H89, but is not dependent on host GPCR-AC, as shown using the inhibitor SQ22536 (see Methods, text and second figure E for details about other inhibitors). Data are mean \pm S.D. of multiple experiments ($n = 2$ in B, C, E and $n = 3$ in A, D).



cell signaling, the underlying mechanism for the cAMP burst remains unclear.⁵⁻⁷ Here, we show that among the 17 adenylate cyclase genes present in *M. tuberculosis*, at least one (Rv0386) is required for virulence. Furthermore, we demonstrate that the Rv0386 adenylate cyclase facilitates delivery of bacterial-derived cAMP into the macrophage cytoplasm. Loss of Rv0386 and the intramacrophage cAMP it delivers results in reductions in TNF- α production via the protein kinase A and cAMP response-element-binding protein pathway, decreased immunopathology in animal tissues, and diminished bacterial survival. Direct intoxication of host cells by bacterial derived cAMP may enable *M. tuberculosis* to modify both its intracellular and tissue environments to facilitate its long-term survival.

Commentary: The present study sheds light on key steps in the *Mycobacterium tuberculosis* (MTB) infection and pathogenesis process which ultimately leads to the establishment of hard-to-eradicate depots of bacteria within the human host. While current antibiotic treatments are successful in killing the circulating MTB, in most patients, there remain bacteria largely contained within granulomas or other types of avascular bodies, where MTB's metabolism is slowed down and converted to hyp-

oxic pathways. Understanding the mechanism of granuloma formation may lead to the design of novel strategies against these latent pools of pathogen. Agarwal and colleagues report the discovery of bacterial adenylate cyclase Rv0386, which was found to be responsible for producing a burst in cyclic AMP (cAMP) upon macrophage infection (see first figure), a process that was shown to require live bacilli but did not involve the host's G-protein coupled receptor adenylate cyclase. The cAMP burst could be modulated by the overexpression of MTB's endogenous phosphodiesterase, thus proving that the responsible agent resides within the bacteria. In a further proof that the cAMP molecules originate from MTB, bacteria grown on ¹⁴C-glycerol were used in an infection experiment and the distribution of radiolabeled cAMP was studied (see second figure). Thus, the study establishes a mechanism whereby MTB takes over the host's cAMP signaling pathway and ultimately influences the host's immune response to its own infection. The high level of TNF- α produced as a result of the cAMP burst triggers an enhanced inflammatory response and the eventual formation of granulomas: the counterintuitive aftereffect of this sequence of events is that MTB conveniently utilizes the granulomas as hiding places. Contributed by Anton Simeonov.



Bacterial-derived cAMP enters the macrophage cytosol after infection. (A and C) Silica gel TLC (A) and PEI cellulose chromatography (C) resolve the nucleotides indicated (ultraviolet visualization). (B and D) After labeling *M. tuberculosis* strains with [¹⁴C]-glycerol, J774 cells infected with the JHU-0386 mutant show significantly reduced bacterial-derived, radiolabelled cAMP in the intramacrophage compartment by silica gel TLC (B) or PEI cellulose separation (D) with autoradiography (top), and densitometric quantification (bottom). WT, wild type. Representative data of several experiments ($n = 2$ in A, C) or mean \pm S.D. ($n = 2$ in B, D) are shown. (E) Pathways of intracellular cAMP intoxication by pathogenic bacteria. This study shows that the *M. tuberculosis* adenylate cyclase Rv0386 is required for the infection-associated macrophage cAMP burst as well as CREB phosphorylation. Red crosses indicate pathways shown not to be involved in the infection-associated cAMP burst. See Supplementary Text 1 for details. AC, adenylate cyclase.

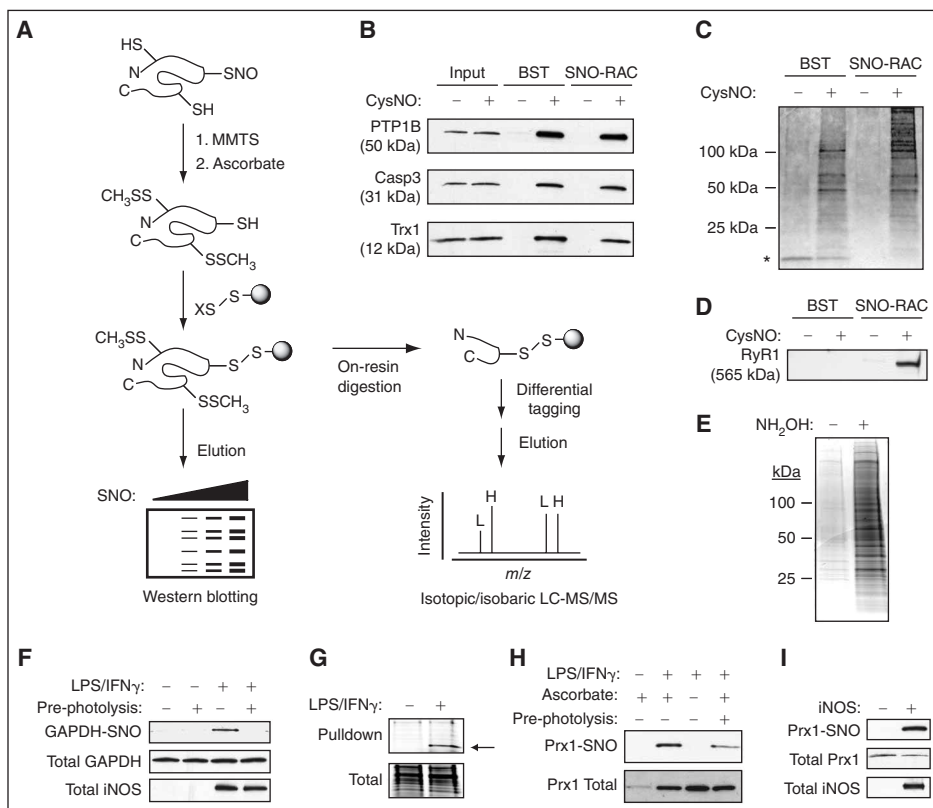
IMPROVED BIOTIN SWITCH TECHNIQUE

Forrester MT, Thompson JW, Foster MW, Nogueira L, Moseley MA, Stamler JS. Proteomic analysis of *S*-nitrosylation and denitrosylation by resin-assisted capture. *Nat Biotech* 2009;27:557–559.

Abstract: We have modified the biotin switch assay for protein *S*-nitrosothiols (SNOs), using resin-assisted capture (SNO-RAC). Compared with existing methodologies, SNO-RAC requires fewer steps, detects high-mass *S*-nitrosylated proteins more efficiently, and facilitates identification and

quantification of *S*-nitrosylated sites by mass spectrometry. When combined with iTRAQ labeling, SNO-RAC revealed that intracellular proteins may undergo rapid denitrosylation on a global scale. This methodology is readily adapted to analyzing diverse cysteine-based protein modifications, including *S*-acylation.

Commentary: It is now well accepted that nitric oxide is a key post-translational modifier of cysteine residues via the process of *S*-nitrosylation. The ways and degrees by which *S*-nitrosylation affects cell signaling continue to be reported and our ability to study this phenomenon relies primarily upon the biotin-switch assay first reported by Snyder and coworkers. The report by Forrester et al provides an improved biotin switch protocol where two steps are conveniently combined. The biotin switch technique involves specific steps of masking and labeling of cysteine residues on proteins in order

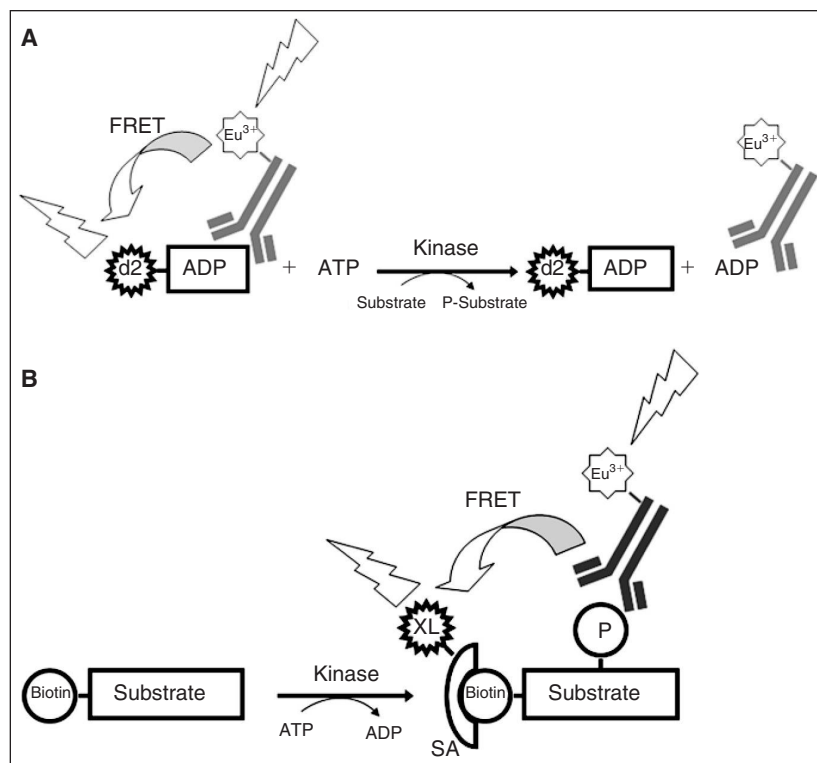


Analysis of protein *S*-nitrosylation by SNO-RAC. **(A)** Protein thiols are blocked with *S*-methylmethanethiosulfonate (MMTS); ascorbate converts SNOs to free thiols; nascent thiols are covalently trapped with a resin-bound 2- or 4-pyridyl disulfide (denoted X); and proteins are eluted with reductant and analyzed by SDS-PAGE. Alternatively, proteins can be trypsinized on-resin to obtain peptides containing SNO sites, which may be differentially "tagged" with isotopic or isobaric mass labels (L, light; H, heavy), and analyzed by MS. **(B and C)** HEK293 cells were incubated in the presence or absence of 0.5 mM CysNO for 10 min and subjected to a side-by-side comparison of the BST and SNO-RAC approaches (1 mg protein per sample). Proteins were separated by SDS-PAGE and visualized by western blotting **(B)** or silver staining **(C)** (see Supplementary Tables 1 and 6 online). Adventitiously eluted streptavidin is indicated by an asterisk. **(D)** Isolated rabbit sarcoplasmic reticulum (1 mg) was treated ± 0.1 mM CysNO for 10 min, subjected to either the BST or SNO-RAC; western blotting was carried out to detect the 565 kDa ryanodine receptor 1 (RyR1). **(E)** Acyl-RAC was performed on HEK293-derived membranes (1 mg protein per sample). Proteins were visualized by SDS-PAGE and Coomassie staining. **(F)** RAW264.7 murine macrophages were treated ± 0.5 mg/mL LPS and 100 U/mL IFNγ to induce inducible nitric oxide synthase, subjected to SNO-RAC (1 mg protein per sample) and analyzed as in c for *S*-nitrosylated GAPDH. Where indicated, extracts were photolyzed to verify assay specificity. **(G–I)** Macrophages were subjected to SNO-RAC (8 mg protein per sample) and eluants visualized by SDS-PAGE and Coomassie staining. The prominent band at B22 kDa was excised and identified by MALDI-MS as peroxiredoxin-1 (indicated by arrow) **(G)**. Lysates (1 mg protein per sample) from stimulated macrophages **(H)** and inducible nitric oxide synthase-transfected HEK293 cells **(I)** were subjected to SNO-RAC and analyzed for *S*-nitrosylated Prx1. For all experiments, $n = 3$. Full-length scans are available in Supplementary Figure 7 online.

to determine the proteins' state of S-nitrosylation: the free unreacted cysteine thiols are first capped with S-methylmethanethiosulfonate and then the S-nitrosylated residues are reduced with ascorbate to uncover the corresponding thiols, which in turn are probed with a biotinylation reagent. The protein, whose formerly S-nitrosylated residues now carry biotin tags, is further analyzed for its biotinylation pattern by streptavidin pull-down. In order to reduce the handling steps, the authors replaced the biotinylation reagent with a thiol-reactive resin: thus, the cysteine thiols liberated after the ascorbate reduction step can be used in a combined tagging and immobilization step, without the need to perform the biotinylation and biotin-streptavidin binding steps (see figure). Comparison analyses of S-nitrosocysteine-treated HEK293 cells revealed identical patterns of S-nitrosylation as determined by the new protocol and the traditional switch technique. Importantly, the resin technique allowed a more sensitive detection of the S-nitrosylation pattern for higher molecular weight proteins (exemplified by the analysis of the 656 kDa ryanodine receptor protein, see figure D). The authors

demonstrate the utility of the SNO-RAC procedure in isolating S-nitrosylated proteins after treatment with an exogenous NO source and following stimulation of inducible nitric oxide synthase (in the latter instance, they identify peroxiredoxin-1 and a substrate for S-nitrosylation). They further show that SNO-RAC easily facilitates trypsin digest and MALDI MS analysis of S-nitrosylated fragments allowing identification of specific cysteine residues that are susceptible to S-nitrosylation. Further, the authors used the new protocol to follow the decrease in S-nitrosylation following a treatment with S-nitrosocysteine and again concluded that the resin protocol was better suited to monitor the dynamic changes in S-nitrosylation patterns proteome-wide. Specific examples like ERK1/2 and PCNA were highlighted to demonstrate the rapid turnover involved in S-nitrosylation/denitrosylation. Given the growing understanding and importance of reactive oxygen species (nitric oxide among them), the advance of the SNORAC process will likely prove to be an important new tool in the biochemist and chemical biologist toolbox. Contributed by Anton Simeonov and Craig Thomas.

HTRF FACEOFF



Hong L, Quinn CM, Jia Y. Evaluating the utility of the HTRF Transcreeper™ ADP assay technology: A comparison with the standard HTRF assay technology. *Anal Biochem* 2009;391(1):31–38.

Principles of the HTRF Transcreeper ADP and standard HTRF kinase assays. (A) HTRF Transcreeper ADP kinase assay. In this assay format, the HTRF Eu donor is labeled on an anti-ADP antibody, whereas the acceptor d2 is labeled on ADP, which serves as a tracer. In the absence of a kinase reaction, the tracer binds to the antibody, resulting in the formation of a FRET pair between the donor and acceptor, leading to high HTRF signal. Kinase-produced ADP competes with the tracer for binding to the antibody, resulting in a loss of HTRF signal. (B) Standard HTRF kinase assay. For a typical assay setup, the substrate is usually biotinylated, facilitating binding to the SAXL acceptor. The Eu donor is labeled on a phospho-specific antibody that binds to the phosphorylation site on the product. Formation of the donor/acceptor complex results in HTRF signal. For both panels A and B, the excitation of the donor molecule at 337 nm results in the FRET transfer to the acceptor molecule at 620 nm, leading to the emission of the acceptor molecule at 665 nm. The ratio of 665/620 nm is recorded as HTRF signal.

LITERATURE SEARCH AND REVIEW

Abstract: The HTRF (homogeneous time-resolved fluorescence) Transcreeper ADP assay is a new kinase assay technology marketed by Cis-Bio International (Bagnols-Cèze, France). It measures kinase activity by detecting the formation of ADP using a monoclonal antibody and HTRF detection principles. In this article, we compare this technology with a standard HTRF kinase assay using EGFR [L858R/T790M] mutant enzyme as a case study. We demonstrate that the HTRF Transcreeper ADP assay generated similar kinetic constants and inhibitor potency compared with the standard HTRF assay. However, the smaller dynamic window and lower Z' factor of the HTRF Transcreeper ADP assay make this format less preferable for high-throughput screening. Based on the assay principle, the HTRF Transcreeper ADP assay can detect both kinase and ATPase activities simultaneously. The ability to probe ATPase activity opens up new avenues for assaying kinases with intrinsic ATPase activity without the need to identify substrates, and this can speed up the drug discovery process. However, caution must be exercised because any contaminating ATPase activity will result in an invalid assay. The inability to tolerate high concentrations of ATP in the assay will also limit the application of this technology, especially in compound mechanistic studies such as ATP competition. Overall, the HTRF Transcreeper ADP assay provides a new alternative tool to complement existing assay technologies for drug discovery.

Commentary: The work by Hong, Quinn, and Jia is a comparison study of the recently developed HTRF Transcreeper ADP assay technology and the traditional HTRF kinase assay. In these HTRF assays, the signal detected is the delayed fluorescence emission resulting from an energy transfer between a long-half-life euro-

pium donor and a red-shifted fluorescence energy acceptor. The principal difference between the two assays is in the analyte being detected: in traditional HTRF, Eu-labeled monoclonal antibody directed at the phosphorylated reaction product is used in combination with streptavidin-coupled fluorescence acceptor which binds to N-terminal biotin placed on the peptide substrate, while in the Transcreeper HTRF, a monoclonal antibody specific for the ADP product (originally developed by Bellbrook Labs as a part of the Transcreeper ADP fluorescence polarization platform) is used in conjunction with acceptor-labeled ADP tracer (see figure). The authors evaluated the two assay platforms with respect to signal window and robustness, as well as in terms of applicability to different needs in kinase inhibitor research. It was found that the traditional HTRF provided higher signal-to-background values and a wider dynamic range; it also allowed direct measurement of ATP K_m and was generally easier to develop as it did not require as much reagent optimization and the generation of calibration curves. The ADP detection method also suffered from its reliance on an imperfect monoclonal antibody whose ADP response was skewed in the presence of high concentrations of ATP. However, the Transcreeper HTRF format was found to be uniquely suited for discovery of inhibitors acting on the ATPase activity of the kinases studied (as many kinases possess ATPase activity, as well), an effect that could not be captured by the regular HTRF assay. In addition, determination of peptide substrate K_m was easier within the Transcreeper format because the peptide was not the molecule being detected in that case. In terms of general robustness and response to inhibitors, both assay platforms performed similarly, indicating that the choice of format will ultimately be guided by the specific needs of the end user. Contributed by Anton Simeonov.

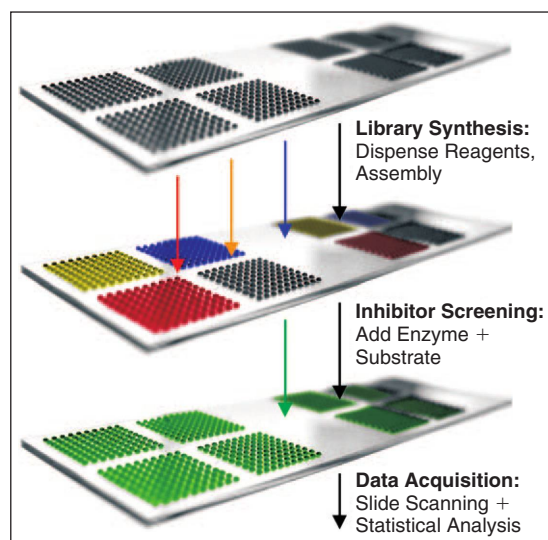
NOVEL SCREENING PLATFORMS: THE TENSION MOUNTS!

Mugherli L, Burchak ON, Balakireva LA, Thomas A, Chatelain F, Balakirev MY. *In situ* assembly and screening of enzyme inhibitors with surface-tension microarrays. *Angew Chem Int Ed Engl* 2009 Jul 6. [Epub ahead of print]

Abstract: Hundreds of reactions were conducted in parallel in droplets maintained on a glass slide through differential surface tension in a new approach to submicroliter-scale synthesis. This "surface-tension microarray" was applied to the *in situ* assembly of thousands of derivatives of phenylboronic acid and their profiling against the NS3/4A protease of the hepatitis C virus. Several potent inhibitors of the enzyme were identified.

Commentary: A familiar issue in drug discovery is that there are more theoretical small drug-like molecules and more biochemical targets than can be examined practically with modern screening tools. Chemists continue to make more molecules and biologists continue to screen more targets, but it remains an overwhelming challenge to assure even modest coverage of chemical and biological space. The most viable solution to these issues continues to be miniaturization. The contribution by Mugherli et al. reports on a nice addition to the field of microarray screening technologies. Using microarrays for small molecule screening is well established. The techniques can be laborious and proper plating of compounds is usually done on the solid array surface. These compounds are

then expected to interact within solution-phase experiments. Here, the authors demonstrate that compounds can be synthesized and evaluated in aqueous phase utilizing previously described microarrays that maintain hydrophilic domains enclosed on a hydrophobic surface (see figure). The synthesis is a straightforward conden-



Conceptual summary of the synthesis and screening of enzyme inhibitors on the surface-tension microarray.

sation of hydrazides with a dialdehyde substrate (DFPB) to yield symmetric and asymmetric dihydrazones. Appropriate controls are reported giving the reader confidence that the novel molecules were indeed created and, importantly, heating was accomplished via microwave irradiation that both facilitates the reaction and the evaporation of the DMSO/glycerol solution. Over 20,000 small molecule dihydrazones were created in this manner and evaluated on the same plates for activity as inhibitors of recombinant NS3/4A protease. The biochemical assay was accomplished in 100 nL water solutions that are held in place via surface tension. Interestingly, the authors demonstrate that Michaelis-Menton enzyme kinetics were observed (an issue for microarray evaluations of small molecules tethered to the solid support). The assay performance was evaluated adjusted for appropriate signal-to-noise ratios and an acceptable Z' factor. The remainder of the manuscript deals with follow-up studies of dihydrazones that were shown to have good inhibitory potential versus the studied protease (one agent was found with an IC_{50} value of 150 nM and showed modest ability to inhibit viral growth in a human cell line). Using microarrays to miniaturize the screening process is not new. However, the ability to synthesize and evaluate novel compounds on a microarray in a fully aqueous environment is an important advance. If these studies can be broadened in terms of chemotypes explored and targets evaluated, the savings in time and resources would be significant. The work by Mugherli et al. demonstrates a first step toward this goal. Contribution by Craig Thomas.